Thermoacoustic Stirling power generation from LNG cold energy and low-temperature waste heat

Kai Wang[a,b], Swapnil Dubey[a], Fook Hoong Choo[a], Fei Duan[b,*]

[a] *Energy Research Institute @ NTU, Nanyang Technological University, Singapore 637141*
[b] *School of Mechanical and Aerospace Engineering, Nanyang Technological University, Singapore 639798*

Abstract

Recovering the cold energy generated in the regasification process of liquefied natural gas (LNG) can help to improve the energy efficiency of LNG power generation systems, meanwhile, abundant low-grade waste heat can also be exploited from the exhaust gas of gas turbines. This study proposes to apply the thermoacoustic Stirling electric generator to recover LNG cold energy and waste heat simultaneously. A pair of linear alternators is directly coupled with the thermoacoustic loop by replacing the long and bulky resonator completely. Numerical simulation is conducted on the basis of the thermoacoustic theory to characterize and optimize the operations of the system. The effects of the back volumes of linear alternators, feedback tube length and regenerator length on the output performances are investigated. The distributions of key parameters, including pressure, volume flow rate, phase difference, acoustic power and exergy flow, are further studied. One design of the thermoacoustic Stirling electric generator operated with 4 MPa helium gas is capable of generating 2.3 kW electric power with the highest exergy efficiency of 0.253 when the cold and hot ends are mantained at 110 K and 500 K. Performances can be further improved if the conversion efficiency of the linear alternators is further increased.

Keywords: Stirling engine, thermoacoustic engine, liquefied natural gas, cold energy, waste heat, linear alternator

---

*Tel: +65 6790 5510; Fax: +65 6792 4062
Email address: `feiduan@ntu.edu.sg` (Fei Duan)

Nomenclature

A	cross sectional area of gas channel, m^2
A_s	cross sectional area of solid, m^2
Bl	force factor, N/A
c_p	gas heat capacity, J/(kg·K)
f	frequency, Hz
f_κ	thermal function
f_ν	viscous function
$\dot{H}_2$	total energy flow, W
I_1	complex electric current, A
k	gas thermal conductivity, W/(m·K)
k_s	solid thermal conductivity, W/(m·K)
K	spring stiffness, N/m
L_e	winding inductance, H
L_{fb}	length of feedback tube, m
L_{REG}	length of regenerator, m
M	moving mass, kg
p_1	complex pressure amplitude, Pa
p_m	mean pressure, Pa
Pr	Prandtl number
$\dot{q}$	heat flux per unit length, W/m
Q_c	cooling power, W
Q_h	heating power, W
r_e	winding resistance, Ω
R_l	load resistance, Ω
R_m	mechanical resistance, N·s/m
T_a	ambient temperature, K
T_c	cooling temperature, K
T_h	heating temperature, K
T_m	mean temperature, K
U_1	complex volume flow rate amplitude, m^3/s
V_b	back volume of linear alternator, m^3
W_a	acoustic power, W
W_e	electric power, W
x	axial coordinate, m
X_1	piston displacement amplitude, m
$\dot{X}_2$	exergy flow, W

Greek letters

γ	specific heat ratio
$\eta_{exe,acoustic}$	exergy efficiency of acoustic power
$\eta_{exe,electric}$	exergy efficiency of electric power
η_{LA}	efficiency of linear alternator
θ	phase difference, rad
ρ_m	mean density, kg/m^3
ω	angular frequency, rad/s

Special symbol

i	notation for a imaginary value
Im[ ]	imaginary part of a complex value
Re[ ]	real part of a complex value
$\|\|$	amplitude of a complex value
$\sim$	conjugate complex

Abbreviations

AHX	ambient heat exchanger
CHX	cold heat exchanger
CTBT	cold thermal buffer tube
HHX	hot heat exchanger
HTBT	hot thermal buffer tube
LNG	liquefied natural gas

1. Introduction

Natural gas is becoming an increasingly important source of energy. About one third of natural gas is traded in the form of liquefied natural gas (LNG) [1], which should be regasificated before further use as the fuel for power generations. Abundant cold energy is generated during the regasification process, while it is typically taken away by seawater in the current industries. Various energy conversion systems have been proposed to recover the LNG cold energy in recent years, such as Rankine cycle, Brayton cycle and combined cycle, etc [2–7].

Stirling cycle heat engines operate with a closed thermodynamic cycle that has the same theoretical efficiency of a Carnot cycle if an ideal regenerator is used [8]. Applying Stirling cycle heat engines for recovering LNG cold energy may provide a good perspective for improving the energy efficiencies for power generation systems [9]. Oshima et al. [10] made a conceptual design of a regasification system for liquid hydrogen or LNG. A cryogenic-type Stirling engine operating between room temperature and the temperature of liquid hydrogen or LNG was proposed to generate electricity from the cold energy. Their results indicated that the Stirling power generation system for cold energy recovery was economically viable. Dong et al. [11] discussed the Stirling cycle for power generation from LNG cold energy. The thermodynamic process and the parameters of the power cycle were analyzed. Szczygieł et al. [12] conducted thermodynamic analyses of a Stirling engine driven by the cold energy of LNG. The effects of the heat transfer temperature, compression ratio and dead volumes ratios on the thermodynamic performance were theoretically investigated. Except for the above conceptual designs and theoretical analyses, several small-scale experimental prototype Stirling engines driven by cold energy were also tested [13, 14]. The generated powers were at the levels of hundreds watts. The drawbacks of the traditional Stirling engines for cold energy utilizations lie in the complicated mechanical moving components at non-ambient temperatures, which introduces great challenges for lubrication and seals, causing instabilities for long-term operations.

Thermoacoustic Stirling engine is a special variant of Stirling engines, which has drawn worldwide interest from both academic and industrial fields in recent years [8, 15–18]. It uses acoustic tubes rather than mechanical pistons to maintain the proper working conditions for the Stirling cycle, resulting in higher reliability, simpler structures and lower costs compared to traditional Stirling engines. One of the promising applications of the thermoacoustic Stirling engine is to generate electricity by coupling acoustic-electric convertors with it. The first thermoacoustic Stirling electric generator was built by Backhaus et al. [19] in 2004, which supplied an electric power of 58 W with a thermal-to-electric efficiency of 15% at the heating temperature of 650 °C. A small thermoacoustic Stirling electric generator with a similar power scale was later developed by Sunpower Inc. [20] by modifying a free-piston Stirling engine. Recently, Wang et al. [21] also developed a small thermoacoustic Stirling electric generator capable of generating 73.31 W. A series of studies were conducted on larger thermoacoustic Stirling electric generators [22–24]. The obtained electric power reached several kilowatts with the highest thermal-to-electric efficiency of about 20% recently. Sun et al. [25] and Wang et al. [26–28] investigated the output characteristics and coupling mechanisms of thermoacoustic Stirling electric generators. The impedance matching between the engine and the linear alternators was found to be critical to the performance. Maximum electric power of about 750 W and a highest thermal-to-electric efficiency of about 16% were reported on an acoustically matched system. A number of thermoacoustic electric generators using low-cost loudspeakers as alternators were built by several other groups and the generated electric powers were within 200 W with efficiencies lower than 5% [29, 30].

All of the above thermoacoustic Stirling electric generators were designed for power generations from high temperature heat sources, i.e. about 400 °C-700 °C. In fact, thermoacoustic Stirling systems are also able to generate useful work at lower temperature ranges. Several thermoacoustic Stirling engines have been successfully developed for generating electricity or cooling power from a low-grade heat at around 100 °C-300 °C recently [31–35]. Among the low-grade heat conversion technologies, organic Rankine cycle systems have been most extensively studied and successfully implemented with powers up to megawatts [36–38]. They have superior efficiencies compared to other technologies for low-grade heat and the ability for scaling up for industrial applications. They require many engineering efforts for the complicated precision moving parts, and therefore are expensive. On the contrary, a recently proposed two-phase thermofluidic oscillator requires little engineering and has few moving parts [39–42]. They have low capital, maintenance and operating costs, however, suffer from low efficiencies. Compared to these technologies, thermoacoustic systems have moderate efficiencies while having the merits of lacking precision mechanical moving components at high temperatures (pistons, turbines, valves, etc.) and the use of inertia working fluids (helium, nitrogen, argon, etc.). They may be a reliable and cost-effective alternative technology for small-scale, distributed applications where the power is at a level of kilowatts.

In addition to high-temperature operations, it is also possible to run a thermoacoustic engine at cryogenic temperatures. For example, a type of thermoacoustic oscillation phenomenon, namely Taconis oscillation, occurs when a transfer line for cryogenic liquid has a large temperature gradient between the ambient and cryogenic temperatures [43, 44]. Wang et al. [45] and Qiu et al. [46] have also experimentally demonstrated that a thermoacoustic engine can be driven by the cold energy of liquid nitrogen. Absent of moving components at cryogenic temperatures are particularly attractive since the cryogenic facilities are always challenge and expensive. Therefore, thermoacoustic systems are capable of full-temperature-range operations for energy conversions.

In gas turbine power stations with LNG as the fuel, aside from the cold energy from the regasification process of LNG, abundant low-temperature waste heat is also available from the exhaust gas of gas turbines. Applying thermoacoustic Stirling engines for recovering LNG cold energy and the waste heat may provide a simply, reliable and efficient solution to improve the overall energy efficiency of the LNG power generation system. In this study, a thermoacoustic Stirling electric generator is presented for simultaneously recovering LNG cold energy and low-temperature waste heat for small-scale LNG power generation systems. Different from the configurations of the previous thermoacoustic Stirling electric generators, the long and bulky resonator is completely replaced by a pair of commercial linear alternators in the proposed system. To assess the performances and provide guidance for future designs, numerical analyses based on the linear thermoacoustic theory are conducted. The effects of key parameters on the performances are numerically investigated. The output characteristics of the thermoacoustic Stirling electric generator are finally studied.

2. System configuration

Fig. 1 illustrates the schematics of the thermoacoustic Stirling electric generator for recovering LNG cold energy and low-temperature exhaust heat. It mainly consists of a thermoacoustic loop and a pair of linear alternators. In a traditional thermoacoustic Stirling engine, a long and bulky resonator is typically used to couple with the loop. Acoustic loads, such as linear alternators or thermoacoustic refrigerators, are usually connected at the junction between the loop and the resonator [27, 28]. In the present design, the resonator is completely replaced by the linear alternators, which eliminates the large acoustic losses in the resonator and makes the whole system more compact. Compared to traditional Stirling engines, the thermoacoustic Stirling electric generator has no mechanical moving components at either cryogenic temperature or high temperature, which makes the system much more reliable. The thermoacoustic loop is mainly composed of a feedback tube, a regenerator, two thermal buffer tubes and four heat exchangers. The LNG cold energy and the low-temperature heat are added at the cold heat exchanger (CHX) and the hot heat exchanger (HHX), respectively. The established temperature gradient along the regenerator enables the working gas in the thermoacoustic system to oscillate spontaneously, converting the thermal energies into acoustic power to drive the linear alternators. Since CHX and HHX are both at non-ambient temperatures, a cold thermal buffer buffer (CTBT) and a hot thermal buffer tube (HTBT) are adopted to isolate them from the other components located at the ambient temperature. At the ambient-temperature ends of CTBT and HTBT, ambient heat exchangers (1AHX, 2AHX) are used. In order to block the harmful acoustic streaming around the thermoacoustic loop, an elastic membrane (not shown in Fig. 1) is installed on the top of 1AHX. The main geometric dimensions of the thermoacoustic loop are listed in Table 1. The linear alternators, just like the resonator in a traditional thermoacoustic engine, should be able to provide enough swept volume flow at the typical working frequencies of around 50-80 Hz in order to successfully couple with the loop. A pair of commercial Qdrive 2s297 linear alternators, which meet the above requirements,

Table 1: Main geometric dimensions of the thermoacoustic loop.

Component	Length (mm)	Diameter (mm)	Notes
1AHX	20	100	porosity: 0.3
CTBT	50	100	
CHX	50	100	porosity: 0.3
Regenerator	Variable	100	porosity: 0.74, 120# stainless steel screen mesh
HHX	100	100	porosity: 0.4
HTBT	270	100	
2AHX	20	100	porosity: 0.3
Feedback tube	Variable	100	

are therefore adopted. The parameters of each alternator are given in Table 2. The coils of the linear alternators are connected in series with a variable electric resistance to extract the electric power.

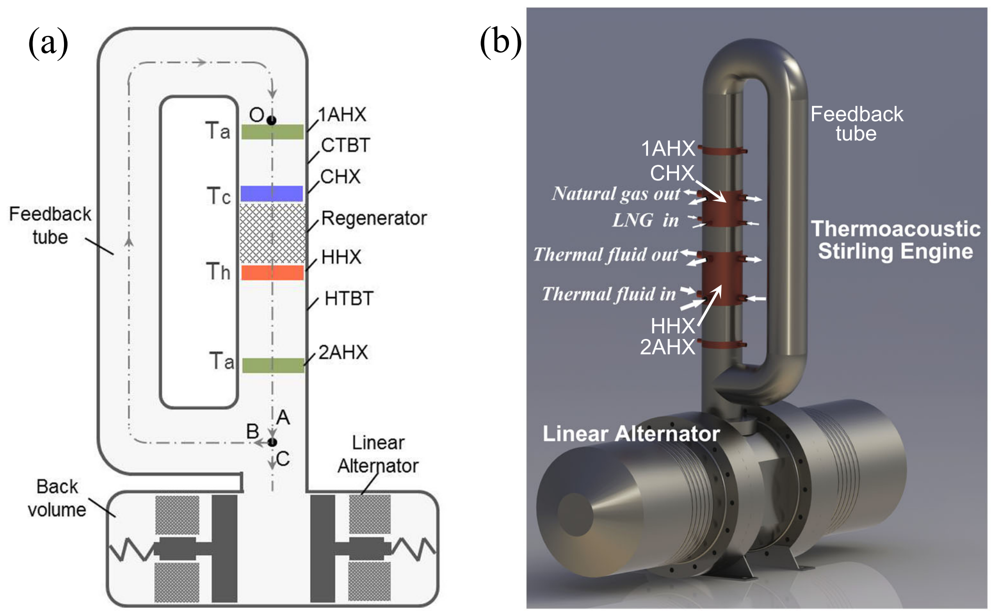

Fig. 1: Schematics of thermoacoustic Stirling electric generator for recovering LNG cold energy and low-temperature waste heat: (a) 2D sketch; (b) 3D drawing.

3. Simulation model

Numerical simulation has been conducted using DeltaEC [47], which is a thermoacoustic simulation platform based on the linear thermoacoustic theory [48]. It has many built-in physical modules for different thermoacoustic components such as ducts, regenerators, heat exchangers and linear alternators, and so on. The physical modules can be arranged and connected in the DeltaEC platform according to the geometric

Table 2: Parameters of the linear alternators (each unit).

Parameter	Value
Winding resistance r_e, Ω	0.5
Winding inductance L_e, mH	12.5
Force factor Bl, N/A	48
Moving mass M, kg	9.307
Spring stiffness K, kN/m	165
Mechanical resistance R_m, N·s/m	50
Piston diameter D, mm	223.3

configuration of the simulated system. The parameters of pressure, volume flow rate, temperature, power, and the others are then numerically calculated after specifying the initial and boundary conditions. DeltaEC has now been widely used for predicting the performances and characteristics of various thermoacoustic systems [29–32, 49–52]. Previous experimental validations of the DeltaEC model for a thermoacoustic Stirling electric generator showed that reasonable accuracies were achieved [26–28]. For example, the relative deviations between simulations and experiments for the electric power typically ranged from 5% to 15% for a thermoacoustic Stirling electric generator with a resonator in Ref. [28]. In Yu et al.'s work about a looped thermoacoustic electric generator [29], the relative deviations were typically in the range of 15%-25%. In the three-stage looped thermoacoustic Stirling electric generator by Bi et al. [24], they were about 30%-55%. The deviations for the thermal-to-electric efficiency were typically around 5% and 8% in Refs. [24] and [28], respectively. The magnitudes of the deviations were influenced by the quality of the developed models and the complexity of the systems. The uncertainties in the present model, which may cause errors of the analyses, result from possibly underestimated or ignored losses from turbulence flow, nonlinear acoustic oscillations, multi-dimensional effects, minor pressure drop, the elastic membrane, heat transfer in the heat exchangers and the regenerator, and so on. Nevertheless, all of the aforementioned work showed that the variation trends of key parameters were well validated, indicating that it is reasonable to identify the critical parameters and provide guidance for future studies on a novel thermoacoustic system based on DeltaEC.

The basic governing equations for the momentum, continuity, and energy in linear thermoacoustic theory are written as follows [48],

$$\frac{\mathrm{d}p_1}{\mathrm{d}x} = -\frac{\mathrm{i}\omega\rho_m}{(1-f_\nu)\,A}U_1 \tag{1}$$

$$\frac{\mathrm{d}U_1}{\mathrm{d}x} = -\frac{\mathrm{i}\omega A}{\gamma p_m}\left[1+(\gamma-1)\,f_\kappa\right]p_1 + \frac{f_\kappa - f_\nu}{(1-f_\nu)\,(1-\mathrm{Pr})}\frac{U_1}{T_m}\frac{\mathrm{d}T_m}{\mathrm{d}x} \tag{2}$$

$$\frac{\mathrm{d}\dot{H}_2}{\mathrm{d}x} = \dot{q} \tag{3}$$

where

$$\dot{H}_2 = \frac{1}{2}\mathrm{Re}\left[p_1\tilde{U}_1\left(1-\frac{f_\kappa-\tilde{f}_\nu}{(1+\mathrm{Pr})\left(1-\tilde{f}_\nu\right)}\right)\right] + \frac{\rho_m c_p|U_1|^2}{2A\omega\left(1-\mathrm{Pr}^2\right)|1-f_\nu|^2}\mathrm{Im}\left(f_\kappa+\mathrm{Pr}\tilde{f}_\nu\right)\frac{\mathrm{d}T_m}{\mathrm{d}x} - (Ak+A_s k_s)\frac{\mathrm{d}T_m}{\mathrm{d}x} \tag{4}$$

The governing equations for a linear alternator are listed as follows,

$$Bl\cdot\frac{U_1}{A} = I_1\left(R_l+r_e+\mathrm{i}\omega L_e\right) \tag{5}$$

$$p_1 A = Bl\cdot I_1 + \left(\mathrm{i}\omega M + R_m - \mathrm{i}\frac{K}{\omega} - \mathrm{i}\frac{\gamma p_m A^2}{\omega V_b}\right)\frac{U_1}{A} \tag{6}$$

The IESPEAKER module is used for the linear alternators in the DeltaEC model.

The exergy flow, $\dot{X}_2$, is calculated by,

$$\dot{X}_2 = \frac{T_a}{T_m}\frac{1}{2}|p_1||U_1|\cos\theta + \left(1-\frac{T_a}{T_m}\right)\dot{H}_2 \tag{7}$$

where θ is the phase difference between p_1 and U_1.

The acoustic power, W_a, is defined as,

$$W_a = \frac{1}{2}|p_1||U_1|\cos\theta \tag{8}$$

The output electric power, W_e, is calculated based on the Joule heating power of the load resistance.

$$W_e = \frac{1}{2}|I_1|^2 R_l \tag{9}$$

It should be noted that the electric current, I_1, is the value when the two linear alternators are connected in series with a load resistance, R_l.

As both cold energy and low-temperature heat are utilized simultaneously in the presented system, the exergy efficiency is more appropriate for evaluating the system efficiency. The exergy efficiency corresponded to the output electric power, $\eta_{exe,electric}$, is calculated by,

$$\eta_{exe,electric} = \frac{W_e}{Q_h\left(1-\frac{T_a}{T_h}\right)+Q_c\left(\frac{T_a}{T_c}-1\right)} \tag{10}$$

where Q_h and Q_c are the heating and cooling powers at HHX and CHX, respectively; T_h and T_c are the temperatures of HHX and CHX, respectively.

The exergy efficiency corresponded to the extracted acoustic power into the linear alternators from the thermoacoustic loop, $\eta_{exe,acoustic}$, is defined by,

$$\eta_{exe,acoustic} = \frac{W_a}{Q_h\left(1-\frac{T_a}{T_h}\right)+Q_c\left(\frac{T_a}{T_c}-1\right)} \tag{11}$$

The efficiency of the linear alternators, η_{LA}, is calculated using,

$$\eta_{LA} = \frac{\eta_{exe,electric}}{\eta_{exe,acoustic}} = \frac{W_e}{W_a} \tag{12}$$

The presented thermoacoustic Stirling electric generator is intended for recovering the cold energy of LNG and the low-temperature waste heat from the exhaust gas of a gas turbine. In the numerical simulations, the solid temperatures of CHX, HHX, AHXs are fixed at 110 K, 500 K and 300 K, respectively. High pressure helium gas is used as the working fluid. The diameter of the thermoacoustic loop is designed uniformly as 100 mm throughout the thermoacoustic loop to minimize the pressure losses related to cross-sectional area changes. In a practical system, the acoustic streaming around the loop is totally blocked by using an elastic membrane. Therefore, it's not necessary to include the acoustic streaming in the model. For simplicity, the loss caused by membrane is ignored here. In the following sections, the effects of the key parameters, including the back volume of linear alternators, feedback tube length and regenerator length, on the operations of the system are investigated. The parametric analyses are conducted in a step-by-step way while considering the parametric interactions and practical restrictions. The distributions of pressure, volume flow and acoustic power, and the output characteristics are then analyzed.

4. Results and discussion

4.1. Effect of back volume

In a traditional thermoacoustic Stirling engine, the long resonator serves as an acoustic inertance, coupling with the loop which behaves as an acoustic compliance. In other words, the resonator is more or less like a moving mass while the loop is similar to a spring. The resonance between the resonator and the loop creates the required acoustic field for the acoustic oscillations and the energy conversions. In the thermoacoustic Stirling electric generator proposed in this study, a pair of linear alternators is coupled with the loop directly. The required acoustic inertance to match the loop is all supplied from the linear alternators. In order to be in the inertance state, the resonant frequency of the linear alternators should be lower than the resulting working frequency of the coupled system. The resonant frequency is mainly determined by the moving mass M, spring stiffness K, and back volume V_b, with the relation of $f = \sqrt{\left(K+\gamma p_m A^2/V_b\right)/M}/(2\pi)$. For the adopted linear alternators, the resonant frequency ranges from 44.3 Hz to 54.5 Hz at 3-5

MPa with the standard back volume of 13.78 L. Since the gas spring is comparable with the mechanical spring in the adopted linear alternators, the resonant frequency can be largely reduced by increasing the back volume. For example, if the back volume is increased to 80 L, the resonant frequency can be reduced to only around 26.6-29.7 Hz.

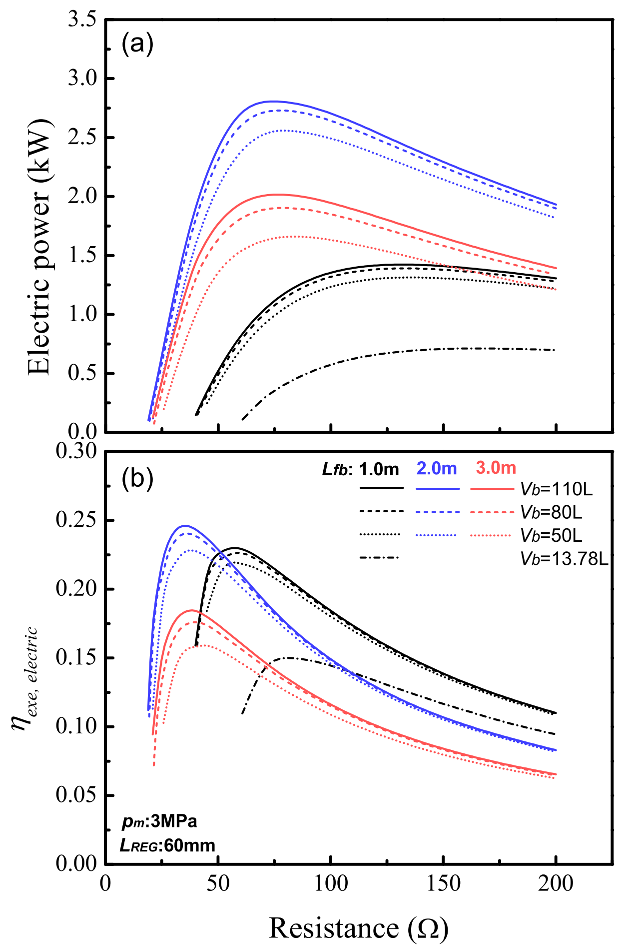

Fig. 2: Effect of back volume V_b on (a) electric power W_e; and (b) exergy efficiency of electric power $\eta_{exe,electric}$.

Fig. 2 shows the effects of the back volume on the electric power and the corresponding exergy efficiency at different feedback tube lengths when the regenerator length is 60 mm. It indicates that both the electric power and the exergy efficiency can be largely increased when the back volume is increased from the standard value to 110 L for any feedback tube length. The influence of the back volume on the performances at larger volumes are relatively weaker compared to those at smaller ones. Besides, it also demonstrates that the feedback tube length has great effects on the performance of the system, and should be optimized. When the feedback tube length is 2 m, the maximum output electric power and the corresponding exergy efficiency reach 2.8 kW and 0.246 respectively with the back volume of 110 L. The same conclusions about the effects of back volume and feedback tube length can be drawn for other regenerator lengths. For simplicity, only the results for the length of 60 mm are shown here. The corresponding displacements of the linear alternators are shown in Fig. 3. The displacement increases with the load resistance for all the feedback tube lengths and back volumes. However, the linear alternators has to be operated within the displacement limit of 13 mm, as denoted by the horizontal dash line in Fig. 3. Therefore, the load resistance should be carefully adjusted to ensure that the displacements are within the safe range. As shown in Figs. 2 and 3, the electric power reaches the maximum value at the displacement of 13 mm when taking the displacement limitation into consideration.

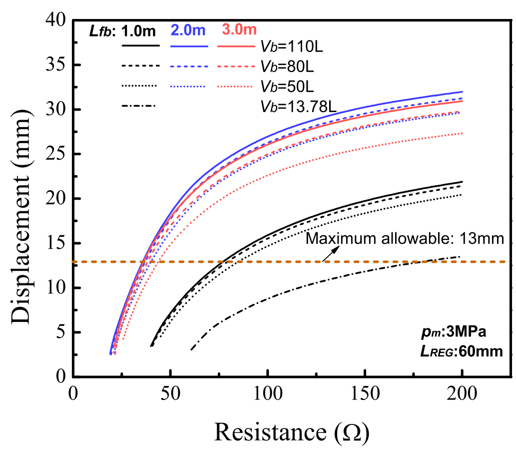

Fig. 3: Effect of back volume V_b on the displacement of linear alternators.

4.2. Effect of feedback tube length

The length of the feedback tube affects the distribution of the acoustic field as well as the phase relation in the regenerator. It is therefore critical for the energy conversion and the dissipations in the thermoacoustic Stirling electric generator. Fig. 4 illustrates the effects of the feedback tube length on the electric power and the exergy efficiency at different back volumes. In the simulations, in order to get the full output capability, the displacement is fixed at the value of 13 mm by adjusting the load resistance, as analyzed in the above section.

It is shown that the feedback tube length has different optimal values for the electric power and the exergy efficiency. The optimal length for the exergy efficiency is slightly lower than that for the electric power. For example, when the back volume is 80 L, the optimal lengths for the electric power and exergy efficiency are 1.73 m and 1.54 m, respectively. The optimal feedback tube lengths are almost the same for different back volumes, showing the weak effects of the back volume on the optimal values. Similar trends are also found for other regenerator lengths.

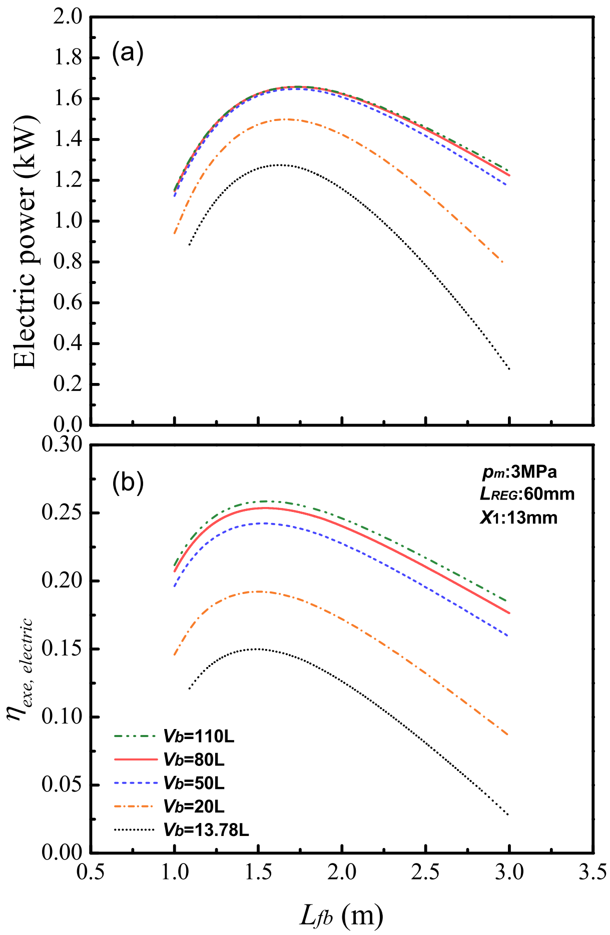

Fig. 4: Effect of feedback tube length L_{fb} on (a) electric power W_e; and (b) exergy efficiency of electric power $\eta_{exe,electric}$.

4.3. Effect of regenerator length

The thermoacoustic energy conversion in the thermoacoustic Stirling electric generator is closely related to the temperature gradient along the regenerator, as indicated mathematically by the temperature gradient terms in Eqs. (2) and (4). As the working temperatures are fixed at 110 K and 500 K, the temperature gradient of the regenerator is determined by the length of the regenerator. As analyzed in Section 4.1, it is beneficial to have a large back volume. The back volume is chosen as 80 L in the following simulations by making a compromise between the performance and the compactness. Optimal exergy efficiency and electric power are obtained by optimizing the feedback tube lengths while fixing the displacement at 13 mm, as analyzed in Section 4.2. The displacement target is reached by adjusting the load resistance accordingly. Fig. 5 shows the optimized exergy efficiency, $\eta_{exe,electric}$, and the corresponding electric power at different regenerator lengths and mean pressures. The output electric power increases when decreasing the regenerator length due to the enlarged temperature gradient. The

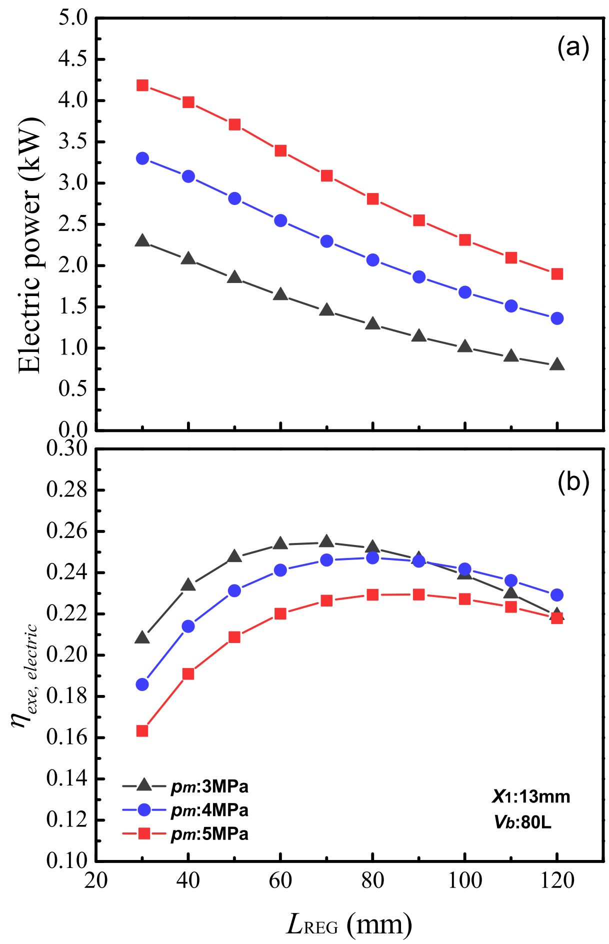

Fig. 5: Effect of regenerator length L_{REG} on (a) electric power W_e; and (b) exergy efficiency of electric power $\eta_{exe,electric}$.

regenerator length should be optimized to get the optimal $\eta_{exe,electric}$. It is beneficial for the output electric power if the mean pressure is increased, while it is basically harmful for $\eta_{exe,electric}$. When the regenerator length is 60 mm with the mean pressure of 3 MPa, the calculated electric power and exergy efficiency are 1.64 kW and 0.254, respectively. When the mean pressure is increased to 5 MPa, the electric power is increased to 3.39 kW, while the exergy efficiency has a slight decrease reaching 0.22.

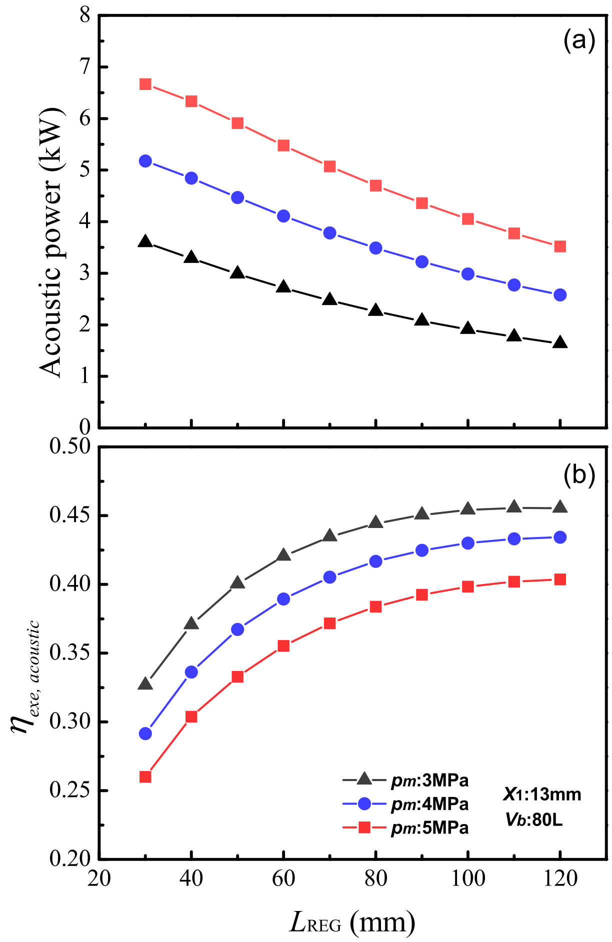

Fig. 6: Effect of regenerator length L_{REG} on (a) output acoustic power W_a; and (b) exergy efficiency of acoustic power $\eta_{exe,acoustic}$.

Fig. 6 illustrates the acoustic power extracted by the linear alternators and the corresponding exergy efficiency, $\eta_{exe,acoustic}$. The acoustic power has similar trends as the electric power. $\eta_{exe,acoustic}$ increases with the regenerator length at the range of interest, and reaches the maximum values at 120 mm. The highest $\eta_{exe,acoustic}$ reaches more than

0.46, showing the good acoustic matching between the thermoacoustic loop and the linear alternators. The obtained $\eta_{exe,acoustic}$ is much higher than $\eta_{exe,electric}$. The reason is that the conversion efficiency of the linear alternators is relatively low mainly due to the large mechanical resistance, as shown in Fig. 7. The highest efficiency of the linear alternators is less than 0.65, and is largely degraded when increasing the regenerator length. If the efficiency of the linear alternators is improved to 0.75, $\eta_{exe,electric}$ is able to reach more than 0.31 at the regenerator length of 60 mm.

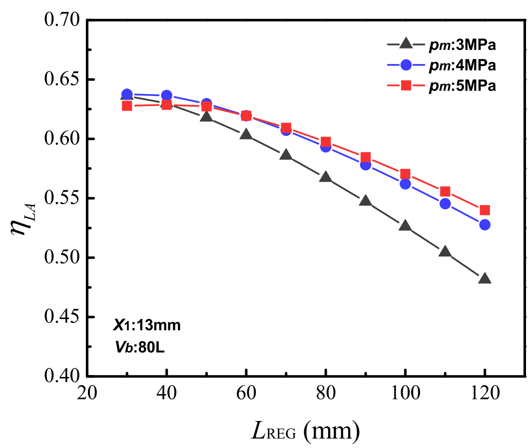

Fig. 7: Effect of regenerator length L_{REG} on efficiency of linear alternators η_{LA}.

The required load resistance and feedback tube length to achieve the optimal $\eta_{exe,electric}$ are given in Fig. 8. The thermoacoustic Stirling electric generator requires larger load resistance to reach the displacement of 13 mm with a longer regenerator. The required load resistance ranges from about 30 Ω to 80 Ω, with smaller values at higher mean pressures. The optimal feedback tube length also increases with the regenerator length. The feedback tube length decreases with the mean pressure for a given regenerator length, resulting in higher working frequencies. The working frequency is at the ranges of 68.2-58.4 Hz for 5 MPa, 61.4-52.5 Hz for 4 MPa, and 53.6-45.6 Hz for 3 MPa respectively when increasing the regenerator length from 30 mm to 120 mm.

4.4. Distributions of key parameters

The distributions of the key parameters along the thermoacoustic Stirling electric generator, including the pressure amplitude, volume flow rate, phase difference, acoustic power and exergy flow, are further investigated to reveal the working characteristics. Fig. 9 shows the distributions of pressure amplitude and volume flow rate when the regenerator length is 70 mm. The mean pressure is set as 4 MPa in the simulation. The feedback tube and the load resistance are optimized to be 1.46 m and 38.6 Ω respectively, as demonstrated in Fig. 8. The working frequency is 56.4 Hz with the given dimensions. The coordinator in Fig. 9 starts from the position O above 1AHX to the tee junction denoted by A, and then back to the position O through the feedback tube, as displayed in Fig. 1(a). The total length of the thermoacoustic loop is 2.12 m. As shown in Fig. 9, the position for the regenerator is highlighted by the gray shadow. The pressure amplitude in the loop ranges from about 0.319 MPa to 0.372 MPa. It has a sharp decrease from 0.372 MPa to 0.328 MPa through the regenerator due to the high viscous resistance. The pressure amplitude reaches the minimum of 0.319 MPa at the tee junction where the linear alternators are connected. With the effect of the acoustic transferring of the feedback tube, the pressure amplitude is then reversed back up to near 0.37 MPa to

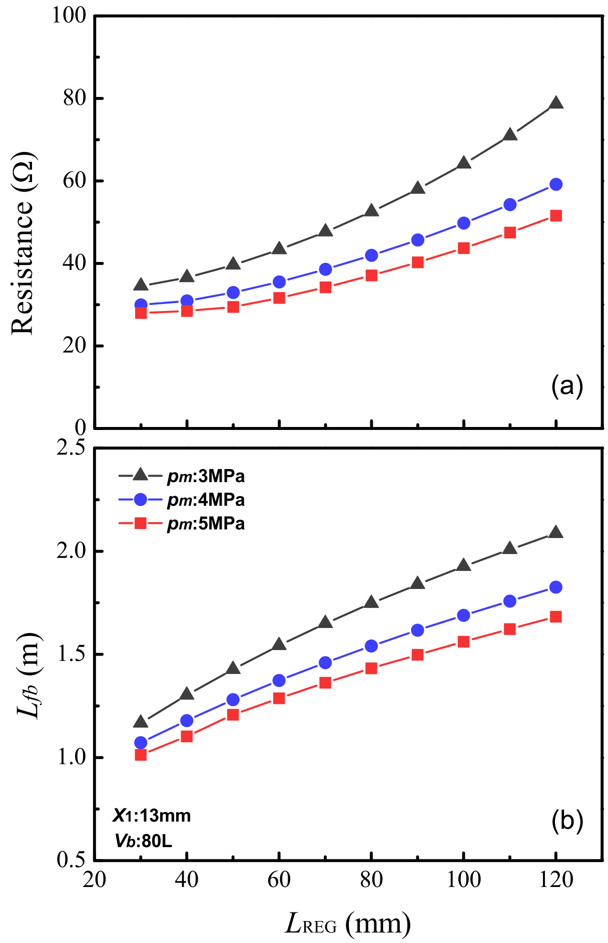

Fig. 8: (a) Optimized load resistance R_l and (b) feedback tube length L_{fb} corresponding to the optimal exergy efficiencies $\eta_{exe,electric}$.

match the acoustic field above 1AHX. The volume flow rate is maintained at a relatively low value of less than 0.05 m^3/s at the regenerator. The achieved low volume flow rate through the regenerator is critical for the high performance of a thermoacoustic Stirling system, since the viscous loss in the regenerator is positively related to the volume flow. The volume flow is branched into three distributaries at the tee junction. The volume flow to the linear alternators is denoted by C. The volume flows into the feedback tube and the energy conversion portion are indicated by B and A, respectively. It indicates that the sum of the volume flows from the loop equals to the one into the linear alternators. Therefore, a large swept volume of the pistons is required for the linear alternators to match the thermoacoustic loop.

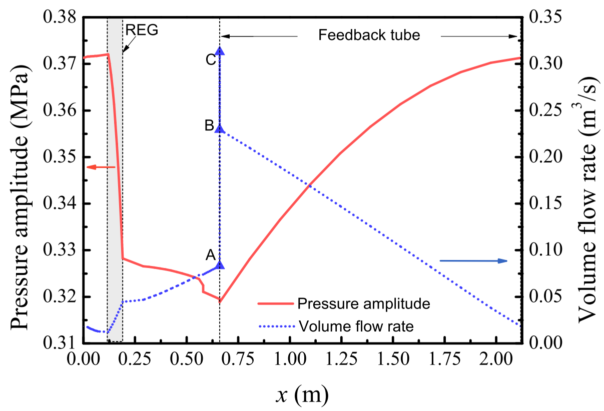

Fig. 9: Distribution of pressure amplitude and volume flow rate along the thermoacoustic loop.

The distributions of the phase difference and the energy flows along the thermoacoustic loop can be seen in Fig. 10. The phase difference ranges from -11.2° to 25.3° from the cold to hot ends. Zero phase difference, i.e. traveling-wave phase, is thus obtained somewhere in the regenerator, which is a good acoustic condition for the Stirling cycle energy conversion. As indicated by C, the phase difference at the tee junction for connecting the linear alternators is 85.5°, which is near a standing-wave phase. This is similar to the acoustic field achieved in the thermoacoustic Stirling engines with long acoustic resonators. The near standing-wave phase results in the requirement of a large volume flow rate for the linear alternators, as analyzed in Fig. 9. A phase reversal changing from a positive value to a negative one occurs at the tee junction. This is because the tee junction is a pressure node and a volume flow antinode. The phase difference along the feedback tube is mainly close to -90°, with a rapid increase to about -48° at the end near 1AHX.

The distribution of the acoustic power clearly shows that it is remarkably amplified by the regenerator. The acoustic power of 2.2 kW flows into the cold end of the regenerator

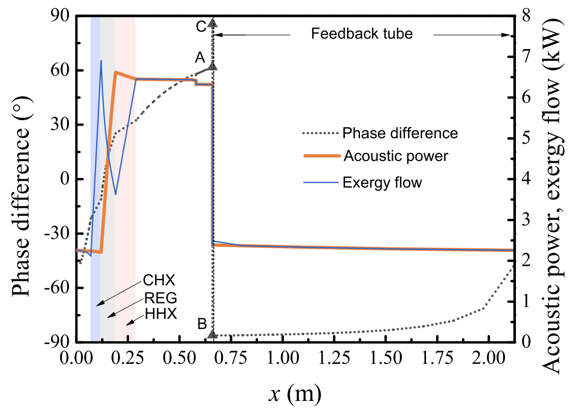

Fig. 10: Distribution of phase difference, acoustic power and exergy flow along the thermoacoustic loop.

and is then amplified to 6.6 kW at the hot end. A large portion of the amplified acoustic power flows into the linear alternators and the rest feeds back into the regenerator through the feedback tube. The large drop of the acoustic power at the tee junction shown in Fig. 10 represents the acoustic power absorbed by the linear alternators, i.e. 3.9 kW, corresponding to 89% of the total generated net acoustic power by the regenerator. By comparison, the power delivered to linear alternators was only about 40% of the total generated acoustic power, while near 35% was dissipated in the resonator in the traditional thermoacoustic Stirling electric generator developed by Wang et al. [27].

The distribution of the exergy flow shows that the exergy is increased in both CHX and HHX due to the added cryogenic exergy of LNG and the exergy of the low-temperarature waste heat, respectively. This is quite different from a thermoacoustic Stirling engine operating between the room temperature and a high temperature, where the exergy flow is only increased at HHX.

4.5. Output characteristics

The output characteristics of the thermoacoustic Stirling electric generator are further analyzed. The geometric and operating parameters are the same as those presented in Section 4.4. Fig. 11 presents the dependencies of the displacement and the working frequency of the system on the load resistance. Similar to the trends in Fig. 3, the displacement increases with the load resistance, and reaches the limit of 13 mm at 38.6 Ω. Therefore, the load resistance should be adjusted within 38.6 Ω for the safety concerns. The curve for the working frequency shows that the system operates almost constantly around 56-57 Hz, which is close to the nominal operating frequency for the linear alternators.

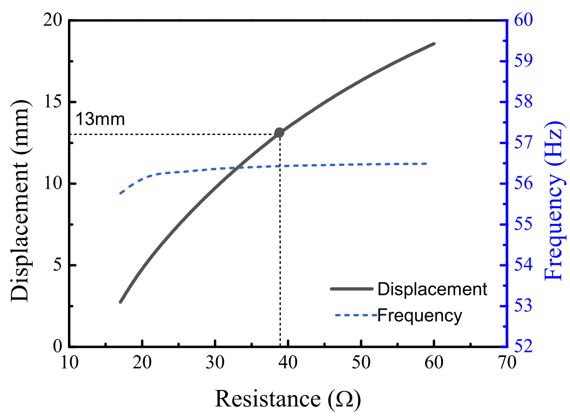

Fig. 11: Displacement and frequency versus load resistance R_l.

The output performances of the thermoacoustic Stirling electric generator with respect to the load resistance are given in Fig. 12. Both the output electric power and acoustic power increase with the load resistance. Considering the limits of the displacement, the adjusting range should be lower than 38.6 Ω, as indicated by the shadow area in Fig. 12. The maximum electric power and acoustic power are 2.3 kW and 3.78 kW, respectively. The exergy efficiencies corresponding to the electric and acoustic powers show that both of them have optimal values. $\eta_{exe,electric}$ reaches the maximum of 0.253 at 30 Ω. The efficiency of the linear alternators demonstrates that it ranges from 0.73 to 0.59 at the operating range, with larger values at lower load resistances.

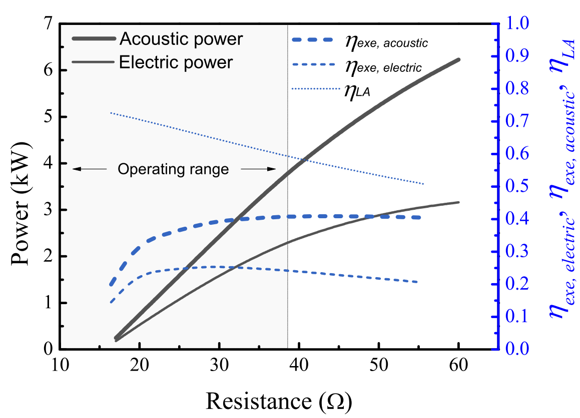

Fig. 12: Output acoustic power W_a, electric power W_e and exergy efficiencies $\eta_{exe,acoustic}$, $\eta_{exe,electric}$ versus load resistance R_l.

The dependencies of the performances on the mean pressure with the displacement at its full load are illustrated in Fig. 13. It shows that the acoustic power and the electric power are both linearly proportional to the mean pressure. When the mean pressure is 5 MPa, the electric power can be increased to more than 3 kW. The obtained $\eta_{exe,electric}$ firstly increases, and then decreases slightly with the mean pressure. $\eta_{exe,acoustic}$, is at the range of 0.41-0.48 when the mean pressure is less than 4 MPa, showing the good energy conversion efficiency of the thermoacoustic engine. The large deviations between the two exergy efficiencies, $\eta_{exe,electric}$ and $\eta_{exe,acoustic}$, are resulted from the low conversion efficiency of the adopted linear alternators since they are originally designed as compressors for cryocoolers. The conversion efficiency of linear alternators can be up to 0.90 provided that they are specifically designed for power generation. In this case, the exergy efficiency of electric power $\eta_{exe,electric}$ of the thermoacoustic Stirling electric generator can be increased to be near 0.40.

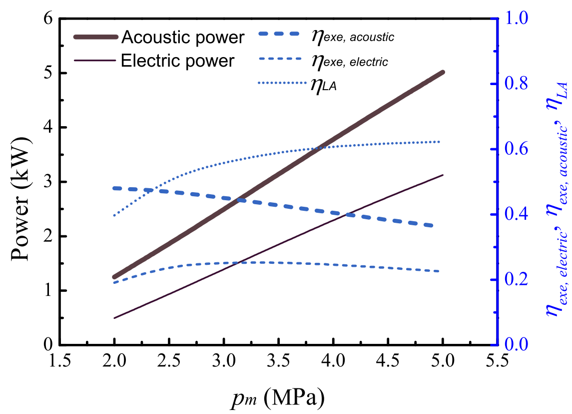

Fig. 13: Output acoustic power W_a, electric power W_e and exergy efficiencies $\eta_{exe,acoustic}$, $\eta_{exe,electric}$ versus mean pressure p_m.

4.6. Comparisons with similar technologies

Compared to traditional thermoacoustic Stirling engines, the proposed thermoacoustic electric generator is much more compact since the long bulky resonator is eliminated. For example, the dimensions of the 1 kW scale traditional thermoacoustic Stirling electric generators developed by Wu et al. [22] and Wang et al. [28] were both about 5 m$\times$1 m$\times$1 m (length$\times$width$\times$height), while it is only about 1 m$\times$1.5 m$\times$1 m for the 2-3 kW system in this work. In the aspect of exergy efficiency, the traditional thermoacoustic Stirling electric generators reached 0.20-0.30 at the heating temperatures of around 650 °C [22, 27]. No work has ever been done on thermoacoustic Stirling electric generators for simultaneously recovering cryogenic cold energy and low-grade heat before. For a fair comparison, when a traditional thermoacoustic Stirling electric generator with a resonator is designed for the same application purpose as that in this study, the predicted exergy efficiency is only 0.17 for the output power of 2 kW based on the similar model, which is much lower than that of the proposed system as analyzed before. This is reasonable, since the resonator dissipates a large portion of the generated acoustic power.

Many large-scale thermodynamic cycles were previously proposed for recovering relative low-temperature waste heat and LNG cold energy. Most of them are based on Rankine cycle or combined cycle, which are usually targeting for providing powers up to megawatts. However, there are also abundant waste heat and cold energy distributed in much smaller scales. The proposed thermoacoustic Stirling electric generator is orientated for these small-scale or portable applications. Compared to the large-scale thermodynamic cycles, the thermoacoustic system is still competitive in the aspect of efficiency. For example, a combined Rankine cycle using LNG cold energy and a heat source at 200 °C reached an exergy of 0.25 [2]. Another combined cycle utilizing LNG and solar energy had an exergy of about 0.23 with the temperature of the collector at 44 °C [36]. Mosaffa et al. showed that a combined organic Rankine cycle for geothermal heat and LNG cold energy had an exergy efficiency of 0.35 at the temperature of 175 °C [37]. In addition to its competitive energy conversion efficiency, the absence of non-ambient temperature moving components and the use of non-corrosive environmentally friendly working fluids make the thermoacoustic Stirling electric generator very reliable and cost-effective for small-scale energy utilization applications.

5. Conclusions

A thermoacoustic Stirling electric generator was proposed for dual-utilizations of LNG cold energy and low-grade waste heat in this work. The system was designed with a compact configuration that the thermoacoustic loop was directly coupled with a pair of linear alternators, totally eliminating the long and bulky resonator in traditional systems. Simulations using DeltaEC software were then conducted to characterize the operations of the system working between 110 K and 500 K. The back volume of the linear alternators and the feedback tube length were critical to the output performances. Increasing the back volume from the standard value of 13.78 L to 80 L was beneficial for both the electric power and the exergy efficiency. The feedback tube length had a great effect on the performances and was optimized. With the regenerator length of 70 mm and the feedback tube length of 1.46 m, the distribution of the acoustic field showed that zero phase difference between pressure and volume flow was achieved in the regenerator. Analysis of the exergy flow indicated that both the cryogenic exergy of LNG and the exergy from low-grade heat were the driving sources for the thermoacoustic Stirling system. The optimized system was able to reach an output electric power of 2.3 kW with the highest exergy efficiency of 0.253 at 4 MPa helium gas. The electric power can be further increased to more than 3 kW by increasing the mean pressure to 5 MPa. This work provides constructive guidelines for designing such thermoacoustic Stirling electric generators. In the near future, an experimental setup for recovering LNG cold energy and exhaust heat from a gas turbine will be built to verify the concept and the predictions.

6. Acknowledgments

The work was funded under the Energy Innovation Research Programme (EIRP, Award No. NRF2013EWT-EIRP001-017), administrated by the Energy Market Authority (EMA). EIRP is a competitive grant call initiative driven by the Energy Innovation Programme Office, and funded by the National Research Foundation (NRF).

References

[1] BP Statistical Review of World Energy 2014. London, UK. BP, 2015.

[2] Kim KH, Kim KC. Thermodynamic performance analysis of a combined power cycle using low grade heat source and LNG cold energy. Appl Therm Eng 2014;70(1):50-60.

[3] Gómez MR, Garcia RF, Gómez JR, Carril JC. Thermodynamic analysis of a Brayton cycle and Rankine cycle arranged in series exploiting the cold exergy of LNG (liquefied natural gas). Energy 2014;66:927-37.

[4] Lin WS, Zhang N, Gu AZ. LNG (liquefied natural gas): A necessary part in China's future energy infrastructure. Energy 2010;35(11):4383-91.

[5] Gómez MR, Gómez JR, López-González LM, López-Ochoa LM. Thermodynamic analysis of a novel power plant with LNG (liquefied natural gas) cold exergy exploitation and CO_2 capture. Energy 2016;105:32-44.

[6] Mehrpooya M, Sharifzadeh MMM, Rosen MA. Energy and exergy analyses of a novel power cycle using the cold of LNG (liquefied natural gas) and low-temperature solar energy. Energy 2016;95:324-45.

[7] García RF, Carril JC, Gomez JR, Gomez MR. Combined cascaded Rankine and direct expander based power units using LNG (liquefied natural gas) cold as heat sink in LNG regasification. Energy 2016;105:16-24.

[8] Wang K, Sanders SR, Dubey S, Choo FH, Duan F. Stirling cycle engines for recovering low and moderate temperature heat: A review. Renew Sustain Energy Rev 2016;62:89-108.

[9] Duan F, Dubey S, Choo FH, Qiu L, Wang K. LNG power generation from gas turbine and Stirling engine. International application No.:PCT/SG2016/050446, 2016 (Filed)

[10] Oshima K, Ishizaki Y, Kamiyama S, Akiyama M, Okuda M. The utilization of LH_2 and LNG cold for generation of electric power by a cryogenic type Stirling engine. Cryogenics 1978;18(11):617-20.

[11] Dong H, Zhao L, Zhang SY, Wang AH, Cai JJ. Using cryogenic exergy of liquefied natural gas for electricity production with the Stirling cycle. Energy 2013;63:10-8.

[12] Szczygieł I, Stanek W, Szargut J. Application of the Stirling engine driven with cryogenic exergy of LNG (liquefied natural gas) for the production of electricity. Energy 2016;105:25-31.

[13] Otaka T, Kodama I, Ota M. Experimental study on a Stirling cycle machine of 100W design capacity. J Power Energy Syst 2008;2(3):1027-35.

[14] Otaka T, Ito M. Operating characteristics of a small cryogenic Stirling engine with a displacer. In: ASME 2011 Power Conference collocated with JSME ICOPE 2011, vol. 2; Denver, Colorado, USA; 2011. p.433-8.

[15] Backhaus S, Swift GW. A thermoacoustic Stirling heat engine. Nature 1999;399:335-8.

[16] Tijani MEH, Spoelstra S. A high performance thermoacoustic engine. J Appl Phys 2011;110:093519.

[17] Yu Y, Sun DM, Wu K, Xu Y, Chen HJ, Zhang XJ, Qiu LM. CFD study on mean flow engine for wind power exploitation. Energy Convers Manag 2011,52(6):2355-9.

[18] Jin T, Huang JL, Feng Y, Yang R, Tang K, Radebaugh R. Thermoacoustic prime movers and refrigerators: Thermally powered engines without moving components. Energy 2015;93(Part 1):828-53.

[19] Backhaus S, Tward E, Petach M. Traveling-wave thermoacoustic electric generator. Appl Phys Lett 2004;85(6):1085-7.

[20] Oriti SM, Schifer NA. Recent Stirling conversion technology developments and operational measurements at NASA Glenn Research Center. In: 7th International Energy Conversion and Engineering Conference (IECEC 2009), Denver, CO, USA; 2009.

[21] Wang YF, Li ZY, Li Q. A novel method for improving the performance of thermoacoustic electric generator without resonator. Energy Convers Manag 2016;110:135-41.

[22] Wu ZH, Zhang LM, Dai W, Luo EC. Investigation on a 1 kW traveling-wave thermoacoustic electrical generator. Appl Energy 2014;124:140-7.

[23] Wu ZH, Yu GY, Zhang LM, Dai W, Luo EC. Development of a 3 kW double-acting thermoacoustic Stirling electric generator. Appl Energy 2014;136:866-72.

[24] Bi TJ, Wu ZH, Zhang LM, Yu GY, Luo EC, Dai W. Development of a 5 kW traveling-wave thermoacoustic electric generator. Appl Energy 2015;185(Part 2):1355-61.

[25] Sun DM, Wang K, Zhang XJ, Guo YN, Xu Y, Qiu LM. A traveling-wave thermoacoustic electric generator with a variable electric R-C load. Appl Energy 2013;106:377-82.

[26] Wang K, Sun DM, Zhang J, Xu Y, Zou J, Wu K, Qiu LM, Huang ZY. Operating characteristics and performance improvements of a 500 W traveling-wave thermoacoustic electric generator. Appl Energy 2015;160:853-62.

[27] Wang K, Sun DM, Zhang J, Xu Y, Luo K, Zhang N, Zou J, Qiu LM. An acoustically matched traveling-wave thermoacoustic generator achieving 750 W electric power. Energy 2016;103:313-21.

[28] Wang K, Zhang J, Zhang N, Sun DM, Luo K, Zou J, Qiu LM. Acoustic matching of a traveling-wave thermoacoustic electric generator. Appl Therm Eng 2016;102:272-82.

[29] Yu ZB, Jaworski AJ, Backhaus S. Travelling-wave thermoacoustic electricity generator using an ultra-compliant alternator for utilization of low-grade thermal energy. Appl Energy 2012;99:135-45.

[30] Kang HF, Cheng P, Yu ZB, Zheng HF. A two-stage traveling-wave thermoacoustic electric generator with loudspeakers as alternators. Appl Energy 2015;137:9-17.

[31] Zhang XQ, Chang JZ. Onset and steady-operation features of low temperature differential multi-stage travelling wave thermoacoustic engines for low grade energy utilization. Energy Convers Manag 2015;105:810-6.

[32] Jin T, Yang R, Wang Y, Feng Y, Tang K. Acoustic field characteristics and performance analysis of a looped travelling-wave thermoacoustic refrigerator. Energy Convers Manag 2016;123:243-51.

[33] de Blok K. Multi-stage traveling wave thermoacoustics in practice. In: The 19th International Congress on Sound and Vibration. Vilnius, Lithuania: International Institute of Acoustics and Vibration and Vilnius University; 2012. p. 1-8.

[34] Senga M, Hasegawa S. Four-stage loop-type cascade traveling-wave thermoacoustic engine. Appl Therm Eng 2016;104:258-62.

[35] Sharify EM, Hasegawa S. Traveling-wave thermoacoustic refrigerator driven by a multistage traveling-wave thermoacoustic engine. Appl Therm Eng 2017;113:791-5.

[36] Rao WJ, Zhao LJ, Liu C, Zhang MG. A combined cycle utilizing LNG and low-temperature solar energy. Appl Therm Eng 2013;60:51-60.

[37] Mosaffa AH, Hasani Mokarram N, Garousi Farshi L. Thermo-economic analysis of combined different ORCs geothermal power plants and LNG cold energy. Geothermics 2017;65:113-25.

[38] Freeman J, Hellgardt K, Markides CN. Working fluid selection and electrical performance optimisation of a domestic solar-ORC combined heat and power system for year-round operation in the UK. Appl Energy 2017;186(Part 3):291-303.

[39] Smith TCB. Power dense thermofluidic oscillators for high load applications. In: 2nd International Energy Conversion Engineering Conference. Providence, Rhode Island, USA: American Institute of Aeronautics and Astronautics; 2004. p. 1-15.

[40] Markides CN, Smith TCB. A dynamic model for the efficiency optimization of an oscillatory low grade heat engine. Energy 2011;36:6967-80.

[41] Kirmse CJW, Oyewunmi OA, Haslam AJ, Markides CN. Comparison of a Novel Organic-Fluid Thermofluidic Heat Converter and an Organic Rankine Cycle Heat Engine. Energies 2016;9(7):479.

[42] Oyewunmi OA, Kirmse CJW, Haslam AJ, Müller EA, Markides CN. Working-fluid selection and performance investigation of a two-phase single-reciprocating-piston heat-conversion engine. Appl Energy 2017;186(Part 3):376-95.

[43] Sun DM, Wang K, Guo YN, Zhang J, Xu Y, Zou J, Zhang XB. CFD study on Taconis thermoacoustic oscillation with cryogenic hydrogen as working gas. Cryogenics 2016;75:38-46.

[44] Gupta PK, Rabehl R. Design guidelines for avoiding thermo-acoustic oscillations in helium piping systems. Appl Therm Eng 2015;84:104-9.

[45] Wang K, Qiu LM, Wang B, Sun DM, Lou P, Rao JF, Zhang XJ. A standing-wave thermoacoustic engine driven by liquid nitrogen. In: Advances in Cryogenic Engineering: AIP Conf Proc 2012;1434:351-8.

[46] Qiu LM, Lou P, Wang K, Wang B, Sun DM, Rao JF, Zhang XJ. Characteristics of onset and damping in a standing-wave thermoacoustic engine driven by liquid nitrogen. Chin Sci Bull 2013;58(11):1325-30.

[47] Ward B, Clark J, Swift GW. Design environment for low-amplitude thermoacoustic energy conversion. Version 6.3b11. Users Guide. 2012.

[48] Swift GW. Thermoacoustics: a unifying perspective for some engines and refrigerators. Sewickley, PA, USA: Acoustical Society of America; 2002.

[49] Xu JY, Hu JY, Zhang LM, Dai W, Luo EC. Effect of coupling position on a looped three-stage thermoacoustically-driven pulse tube cryocooler. Energy 2015;93(Part 1):994-8.

[50] Zhang S, Wu ZH, Zhao RD, Dai W, Luo EC. Numerical investigation on a thermoacoustic heat engine unit with a displacer. Energy Convers Manag 2014;85:793-9.

[51] Zhao Y, Yang Z, Luo EC, Zhou Y. Travelling-wave thermoacoustic high-temperature heat pump for industrial waste heat recovery. Energy 2014;77:397-402.

[52] Al-Kayiem A, Yu ZB. Numerical investigation of a looped-tube travelling-wave thermoacoustic engine with a bypass pipe. Energy 2016;112:111-20.